Central European Journal of Energetic Materials
ISSN 1733-7178; e-ISSN 2353-1843

Cent. Eur. J. Energ. Mater. 2020, *17*(1): 85-106; DOI 10.22211/cejem/118837
Article is available in PDF-format, in colour, at:
http://www.wydawnictwa.ipo.waw.pl/cejem/Vol-17-Number1-2020/CEJEM_01032.pdf

Research paper

Effect of Drying Conditions on the Characteristics and Performance of B/Fe_2O_3 Nano-Composites Prepared by Sol-Gel Method

Nil Ezgi Dinçer Yilmaz[1,*], Gürkan Karakaş[2]

[1] *Roketsan Inc, Ankara, PO Box 30, Turkey*
[2] *Middle East Technical University, Ankara, 06800, Turkey*
* *E-mail:* edincer@roketsan.com.tr

Abstract: B/Fe_2O_3 samples were prepared by mixing nano sized boron powder with iron oxide xerogels that had been synthesized using a sol-gel method that included various types of proton scavengers such as 1,2-epoxybutane, tetrahydrofuran, 1,4-dioxane and ammonium hydroxide. The effects of the proton scavengers and drying conditions on the textural properties of the iron oxide samples and on the heat output and thermal behavior of the nano-composites were examined. The iron oxide samples were subjected to direct drying (DD) or sequential solvent exchange (SSE). The heat output values of the B/Fe_2O_3 nano-composites varied from 240 to 1200 J/g depending on the drying condition and the proton scavenger used. It was found that the thermal behaviour and the textural properties of B/Fe_2O_3 nano-composites (such as porosity, surface area and crystallinity) could be tailored by both the drying conditions and the proton scavenger used.

Keywords: nano-composite, pyrotechnic, sequential solvent exchange, proton scavenger, heat output, energetic materials, boron

1 Introduction

The pyrotechnic compositions used in initiator systems are generally activated by a specific well defined electrical impulse. These initiators are used in both civilian and military systems as gas-generators, igniters, microelectromechanical systems (MEMS)-based microthruster systems and also in initiators for automobile airbags [1-3].

The pyrotechnic compositions may be prepared by various methods such as physical mixing, arrested reactive milling and the sol-gel method [4, 5]. The sol-gel method is a versatile synthesis technique to produce energetic materials and oxidizers. It is a well-known technique for the production of nano-structured pyrotechnic materials [6-9]. This method is safe for the processing of energetic materials at room temperature and low temperature drying. The methodology is based on the synthesis of nanoparticles by the reaction of components in a solution which is called 'sol' and then by linking them together in a solid matrix called 'gel' with a porous structure [4]. Following the synthesis of gel form when the liquid phase is removed from the gel by controlled evaporation, high density and porous xerogels are obtained. These xerogels have nanometer size particles and pores. The sol-gel methodology provides intimate mixing and contact of the components. It is rather an easy way to control and tailor the properties of energetic material with the possibility of achieving ultrafine particle dispersion which is not practical by conventional methods [6]. The new applications of this well-known method are developing self-assembled nanocomposites [10, 11] and penetration of oxidizer through the silicon substrates [12-14].

This is an example of the "bottom-up" concept that was first brought to prominence with Richard Feynman's talk, "There's Plenty of Room at the Bottom" at the American Physical Society Meeting in 1959 [15]. Since that time, the field of nanoparticles has grown and improved with many research studies published. However, the application of nanotechnology to energetic compositions is a new topic and it seems that nano-sized energetic materials will become the next-generation of energetic materials due to their controllable surface area, energy density, particle size distribution and power/heat release.

Pyrotechnics exhibit highly exothermic oxidation-reduction reactions between the oxidizer and the fuel [16]. The sol-gel method offers good control of the textural and structural properties of the metal oxides. The particle size, porosity, surface area and crystallinity of the metal oxides can be tailored by the synthesis and drying conditions [4, 17-19]. These structural properties

have great importance for the ignition and combustion performance of energetic compositions.

The morphological and structural properties of the oxidizer affect the combustion characteristics of the energetic nano-composites depending on the particle size, surface area and porosity of the components. A limited number of studies have been reported that consider the effect of textural properties on ignition and combustion performance [5-9, 20-24]. In these studies, significant changes in ignition and combustion performance were observed for energetics with 100 nm or smaller particle size. The small particle size, the resulting higher surface area, and the intimate contact between particles produce a decrease in the mass transport distance between the fuel and oxidizer [20, 25]. The pyrotechnics that include nano oxidizer and fuel can be defined as nano-composite pyrotechnics, metastable intermolecular/ interstitial composites (MICs) or superthermites [26]. The application of nano energetics to MEMS technology may lead to size and mass reductions of many munitions systems in the future [3].

The initial combustion reactions in a binary fuel-oxidizer system of thermites/ pyrotechnics are assumed to be controlled by transport processes, such as mass diffusion and heat transfer between the component particles [22, 27]. Heat transfer is produced only by heat conduction in non-porous structures. For efficient combustion the heat transfer mechanism should involve both conduction and convection. Therefore, porous structures are necessary for an efficient and uniform combustion *via* heat convection and conduction mechanisms. In addition, the oxide layer around the fuel particles acts as a passivation layer to protect/isolate them from their surroundings. Oxygen must diffuse through this passivation layer from the oxidizer in order to directly contact the fuel particles. Thus the mass diffusion between the oxidizer and the fuel acts as a rate controlling step for the combustion reaction of pyrotechnics [28, 29]. Since pyrotechnic reactions are diffusion-limited processes, a higher surface area facilitates uniform combustion and enhances the combustion performance of the thermites/pyrotechnics. The particle size and the surface area of metal oxides synthesized by the sol-gel method depends strongly on the drying conditions and the proton scavenger used. The strong interaction between the polar solvent residues and the metal oxide gel requires elevated drying temperatures. It is known that the direct drying (DD) process leads to the formation of capillary forces inside the pore walls of the gel structure and this capillary force results in shrinkage and collapse of the gel matrix. In order to prevent shrinkage, solvent exchange could be applied in which polar solvent residues are exchanged with non polar solvents prior to drying.

Therefore, the solvent exchange method provides better control of surface area and porosity, avoiding contraction of the matrix.

In this present study the effect of proton scavengers (used to initiate the gelation mechanism of the precursor, $Fe(NO_3)_3 \cdot 9H_2O$) on the textural properties of the iron oxide samples and the influence of the type of proton scavenger on the heat output were investigated. The energetic performance of sol-gel synthesized Fe_2O_3 was examined in Fe_2O_3-boron pyrotechnic reactions which can be described by Equation 1 [30]:

$$2B + Fe_2O_3 \rightarrow B_2O_3 + 2Fe \qquad \Delta H = -2473 \text{ J/g} \qquad (1)$$

The effect of solvent exchange on the textural properties and thermal behavior of B/Fe_2O_3 nano-composites was also studied.

2 Materials and Methods

2.1 Materials

Iron(III) nitrate nonahydrate ($Fe(NO_3)_3 \cdot 9H_2O$, ≥99.8%, Sigma Aldrich) was used as precursor. Ethanol (≥99.8%, Sigma Aldrich) was used as solvent. 1,2-Epoxybutane (99%, Aldrich), tetrahydrofuran (THF, anhydrous, 99.9%, Sigma Aldrich), 1,4-dioxane (anhydrous, 99.8%, Sigma Aldrich) and ammonium hydroxide solution (28% NH_3 in H_2O, Sigma Aldrich) were used as proton scavengers. Boron powder (≥98.5%) with an average particle size of 200 nm was provided by a local supplier and used as fuel. All materials were used in their as received conditions.

2.2 Synthesis of iron oxide samples

Iron oxide samples were synthesized by the sol-gel method. 4.0 g of $Fe(NO_3)_3 \cdot 9H_2O$ was hydrolyzed in 6.4 cm^3 of ethanol producing a clear red-orange solution in a glass beaker that was constantly stirred at 400 rpm using an explosion proof magnetic stirrer (2 mag magnetic motion atexMIXdrive 1) under ambient conditions. After hydrolysis, gelation was carried out by the slow addition of one of the proton scavengers to the solution. In all synthesis work, 64.6 mmol of the proton scavenger was used except 1,4-dioxane (32.3 mmol) and ammonium hydroxide solution (128 mmol). The samples were dried by conventional oven drying method at 70 °C for 6 days to remove the solvent and other volatiles. The solvent exchange method was used to remove the residual ethanol and other volatiles by successive treatment of the gel sample

by a series of ethanol-hexane mixtures containing 25, 50 and 75 wt.% hexane. The gel samples were treated with each solvent mixture for 3 days at room temperature and the solvent was drained completely after each step. The solvent exchange process was followed by drying of the samples at 90 °C overnight.

2.3 Preparation of boron/iron oxide energetic composites

B/Fe_2O_3 composites were obtained by physical mixing of specific amounts of boron powder with iron oxide samples that had been prepared *via* the sol-gel method. The compositions have a specific mass ratio which can be described as an equivalence ratio. The equivalence ratio is the ratio of the actual mass ratio of fuel to oxidizer to the stoichiometric mass ratio of fuel to oxidizer. It is calculated by using the main chemical reaction between the boron and iron oxide (Equation 1) as Equation 2:

$$\phi = \frac{\left(\mathbf{m_{fuel}}/\mathbf{m_{oxidizer}}\right)_{\mathbf{actual}}}{\left(\mathbf{m_{fuel}}/\mathbf{m_{oxidizer}}\right)_{\mathbf{stoichiometry}}} \quad (2)$$

The B/Fe_2O_3 samples subjected to thermal analysis were fuel rich compositions. The equivalence ratio of the samples is given in Table 1. The equivalence ratios take into account that 2 moles of B should be added to 1 mole of Fe_2O_3 or 2 moles of $Fe(NO_3)_3 \cdot 9H_2O$ for a stoichiometric reaction. Therefore, for a 3FR composition, 6 moles of B should be added to 1 mole of Fe_2O_3 or 2 moles of $Fe(NO_3)_3 \cdot 9H_2O$.

Table 1. Fuel and oxidizer content of B/Fe_2O_3 nano-composites

Sample	B content [mmol]	Fe_2O_3 content [mmol]	Equivalence ratio, φ
3FR	6	1	3

3 Material Characterization

3.1 Nitrogen gas adsorption analysis

The textural properties of the iron oxide samples synthesized *via* the sol-gel method using various proton scavengers were examined using the N_2-BET method. The nitrogen adsorption-desorption isotherms of the samples were analyzed with a Quantachrome Autosorb-6iS Instrument. The samples were degassed at 200 °C for a minimum of 24 h under vacuum. The surface area, pore size

distribution and pore volume were determined by the nitrogen adsorption-desorption isotherms.

3.2 X-Ray diffraction (XRD)

The X-ray diffraction (XRD) analysis of Fe_2O_3 samples were performed at room temperature by Rigaku ULTIMA IV X-ray diffractometer using monochromatic CuKα X-Rays with a wavelength of 0.15405 nm between 2θ range of 3-90° with a scan speed of 0.5°/min and a sampling step of 0.02°. Database PDF-2 from ICDD was used to specify the lattice structures and phases.

3.3 Thermal analysis

The thermal analyses of B/Fe_2O_3 compositions were carried out using a NETZSCH STA 449 F3 Simultaneous TG-DSC analyzer to characterize the onset temperature and energy release of the samples. TG-DSC measurements were performed by loading 1.5-2.0 mg of samples into Al_2O_3 crucibles and heating from room temperature up to 1400 °C at a heating rate of 30 °C/min with an accuracy of 0.0001 mg. The measurements were performed under a high purity (99.999%) nitrogen atmosphere.

4 Results and Discussion

4.1 Nitrogen gas adsorption analysis

In this study, the effect of proton scavenger, solvent exchange and drying conditions on the textural properties were examined using the N_2-BET method. The adsorption-desorption isotherms and pore size distribution of Fe_2O_3 samples are presented in Figures 1 and 2, and Table 2. The samples prepared by the sequential solvent exchange (SSE) and DD methods exhibit a Type IV isotherm with a hysteresis loop which indicates a mesoporous structure [31-33]. The hysteresis loops over the relative pressure of 0.5 indicate the presence of mesopores in the skeletal matrix.

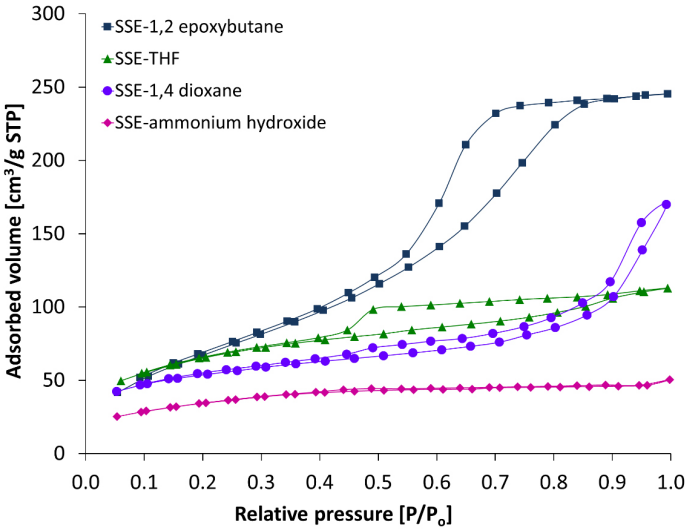

(a)

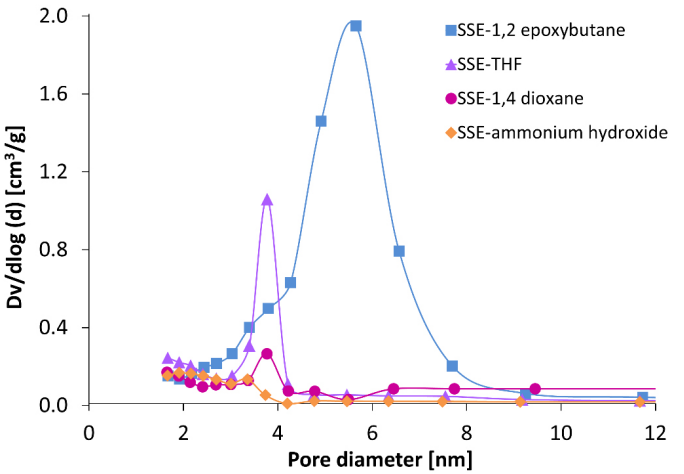

(b)

Figure 1. SSE Fe_2O_3 samples synthesized with 1,2-epoxybutane, THF, 1,4-dioxane, ammonium hydroxide: (a) the nitrogen adsorption/desorption isotherms and (b) the pore size distributions

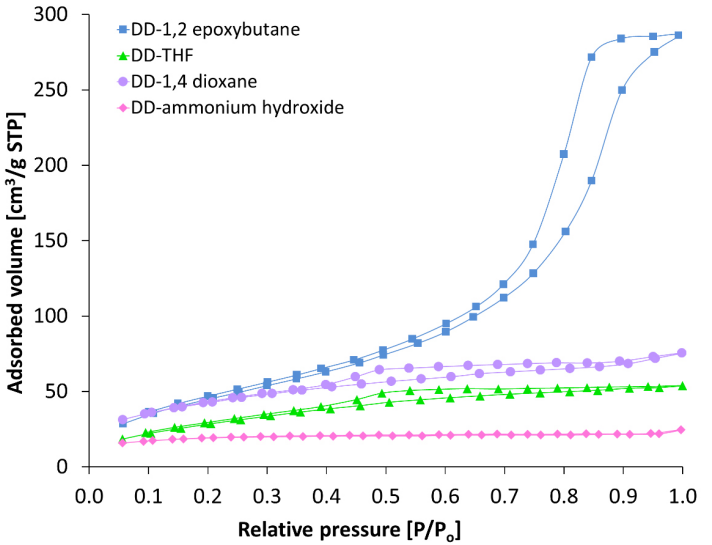

(a)

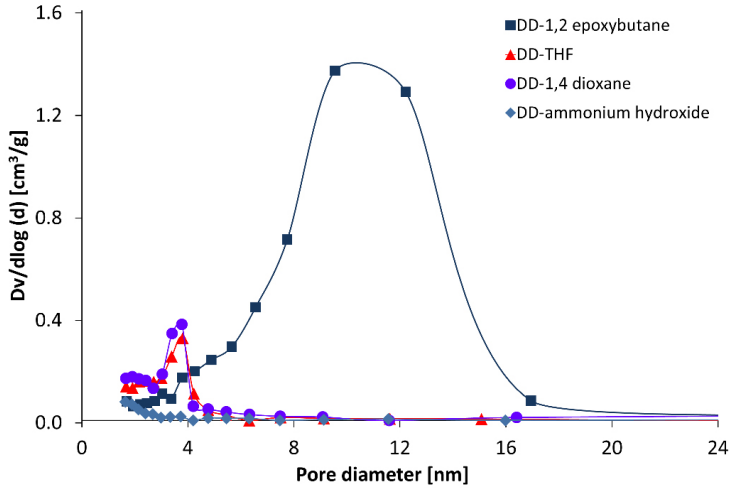

(b)

Figure 2. DD Fe_2O_3 samples synthesized with 1,2-epoxybutane, THF, 1,4-dioxane, ammonium hydroxide: (a) the nitrogen adsorption/desorption isotherms and (b) the pore size distributions

Table 2. The surface area, pore size and pore volume of Fe_2O_3 compositions

Proton scavenger	Surface area [m^2/g]		Pore volume* [cm^3/g]		Average pore diameter* [nm]	
	DD	SSE	DD	SSE	DD	SSE
1,2-Epoxybutane	176.2	267.6	0.462	0.432	9.553	5.653
THF	109.1	231.7	0.087	0.179	3.804	3.776
1,4-Dioxane	150.9	190.5	0.103	0.427	3.406	1.654
Ammonium hydroxide	67.1	123.3	0.022	0.063	1.646	1.664

* The pore volumes and the average pore diameter were obtained from nitrogen desorption isotherms by the BJH theory

The specific surface area, pore volumes and average pore diameter of the iron oxide samples prepared using the DD method varied between 67-176 m^2/g, 0.022-0.462 cm^3/g and 1.646-9.553 nm, respectively. On the other hand, the specific surface area and the pore volume of the samples prepared by the SSE method were significantly higher than the samples prepared by the DD method. The specific surface area, pore volumes and average pore diameter of the iron oxide samples prepared by SSE varied between 123-268 m^2/g, 0.063-0.432 cm^3/g and 1.654-5.653 nm, respectively. The wide range in the surface area can be explained by the different mechanisms, which follow through during the gelation process, depending on the proton scavenger used.

The results show that the iron oxide samples synthesized by the sol-gel method were in the xerogel form having mesoporous structures except for the samples synthesized using ammonium hydroxide and subjected to the DD method. The evaporation of the ethanol and other volatiles from the gel sample by direct drying led to excessive capillary forces on the gel's pore structure and these capillary forces resulted in shrinkage of the gel matrix. Besides, the solvent removal rate and drying is favored by the presence of non polar solvent and the porous structure was preserved after drying at 90 °C.

The sample prepared using ammonium hydroxide resulted in the smallest surface area and pore volume, because the ammonium hydroxide is more basic compared to other proton scavengers. As a result, the rapid precipitation of Fe_2O_3 phase and crystallization process may lead to destruction of the porous structure. However, the particle size, porosity, surface area and crystallinity of the iron oxide can be tailored by the synthesis and drying conditions.

4.2 X-Ray diffraction (XRD)

XRD patterns of iron oxide samples which were synthesized using various proton scavengers and which were prepared by both the DD and SSE methods are given

in Figure 3. The broad peaks of the samples prepared with 1,2-epoxybutane, THF and 1,4-dioxane may be attributed to the structure of the maghemite phase of γ-Fe_2O_3 according to PDF card no 00-004-0755 of the ICDD database as shown in Figure 3.

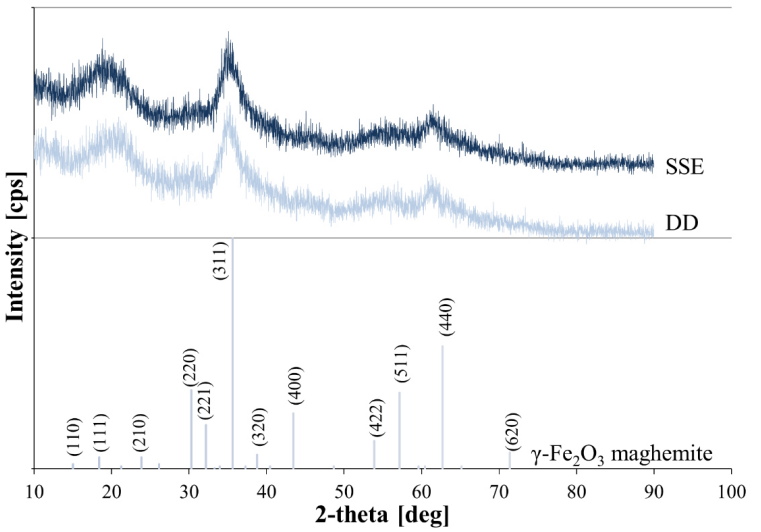

(a)

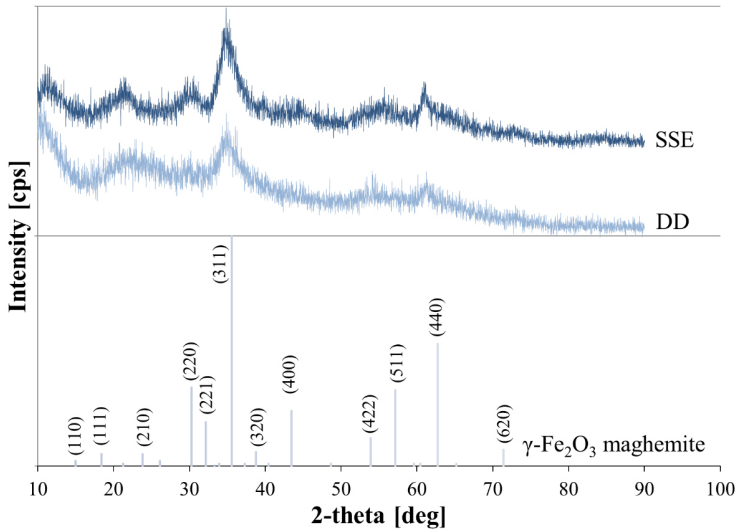

(b)

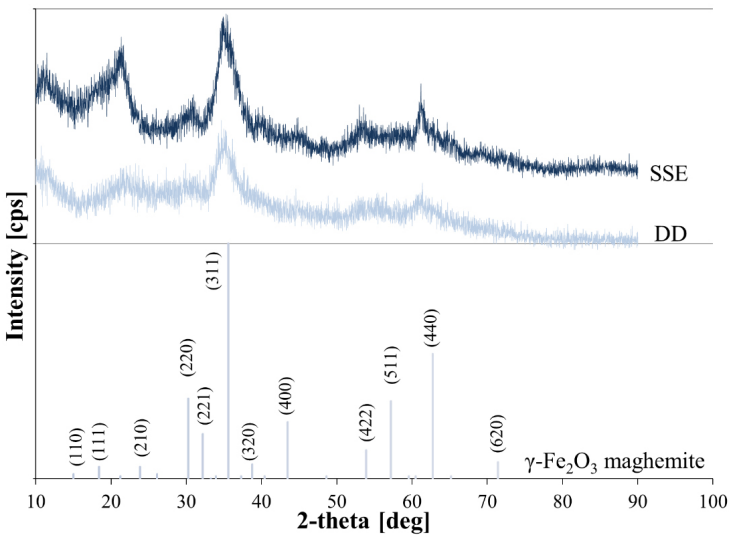

(c)

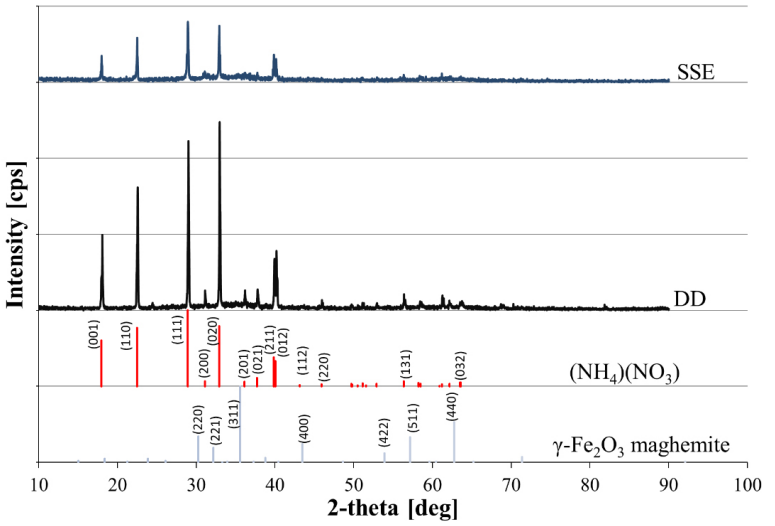

(d)

Figure 3. The XRD patterns of DD and SSE Fe_2O_3 samples synthesized with (a) 1,2-epoxybutane, (b) THF, (c) 1,4-dioxane, and (d) ammonium hydroxide

The spinel structure of γ-Fe_2O_3 consists of layers of tetrahedral and octahedral positions [18, 34] and Fergusan *et al.* [35] indicated that the octahedral sites of maghemite involve cation vacancies. These cation vacancies are important for the iron oxide which is used as an oxidizer in pyrotechnic compositions. The pyrotechnic reactions are based on the oxidation-reduction mechanism between the iron oxide and the fuel used in the compositions and the existence of these cation vacancies affect the structural properties of the iron oxide xerogels and as a result they also affect the pyrotechnic reaction mechanism [36]. Moreover, the pyrotechnic reaction threshold is influenced by changes in the crystal structure and the lattice defects of the iron oxide xerogel [37-39].

The peaks observed at $2\theta = 20°$ for samples prepared with epoxybutane, THF and 1,4-dioxane (Figures 3(a)-(c)) indicate a super lattice structure with the ordering of cation vacancies in the maghemite crystal lattice which is specific to sol-gel synthesized samples. The intensity of these diffraction peaks was found to be relatively small presumably because of the lower crystallinity of the xerogel structure [34, 40-43].

On the other hand, the XRD patterns of the sample synthesized using ammonium hydroxide are different from those of the samples synthesized with other proton scavengers as shown in Figure 3(d). The sharp peaks of the sample synthesized using ammonium hydroxide may be attributed to the structure of residual ammonium nitrate (NH_4NO_3). The presence of NH_4NO_3, presumably arises from the reaction of free NO_3^- ions which are generated during the hydrolysis step of $Fe(NO_3)_3 \cdot 9H_2O$ as given in the following Equations 3 and 4. The other peaks of the sample synthesized using ammonium hydroxide may be attributed to the maghemite phase of γ-Fe_2O_3 according to PDF card no 00-004-0755 of the ICDD database.

$$Fe(NO_3)_3 \cdot 9H_2O \rightarrow Fe(NO_3)_3 + 9H_2O \quad (3)$$

$$Fe(NO_3)_3 + 3NH_4OH + 9H_2O \rightarrow 3NH_4NO_3 + Fe(OH)_3 + 9H_2O \quad (4)$$

XRD patterns of samples synthesized with ammonium hydroxide and prepared by the DD and SSE methods consisted of similar sharp peaks attributed to the residual NH_4NO_3. However, XRD patterns of samples synthesized using epoxybutane, THF and 1,4-dioxane and prepared by the DD method are very similar to those of samples obtained by the SSE method except for a slight increase of peak intensity after sequential solvent exchange which can be explained by Ostwald ripening during solvent exchange. The nano-scale structures of the iron oxide utilized as the oxidizer resulted in a higher

mass transport rate which is known as the controlling step of the pyrotechnic combustion reaction.

Based on the XRD patterns of iron oxide samples synthesized using 1,2-epoxybutane, THF and 1,4-dioxane and prepared by the DD and SSE methods, the crystallite size (L), was calculated from the (311) XRD peak which is common to γ-Fe_2O_3 (maghemite) using the Scherrer equation [44, 45]:

$$L = \frac{K\lambda}{\beta cos(\theta)} \tag{5}$$

where K is a constant related to crystallite shape (0.94), λ is the X-ray wavelength (0.15405 nm for CuKα), β is the full width at half maximum (FWHM) of (311) γ-Fe_2O_3 diffraction maximum in radians and θ is the diffraction angle. The calculated values on the basis of Equation 5 may be considered as a preliminary measure of the crystallite sizes of iron oxide xerogels synthesized with 1,2-epoxybutane, THF and 1,4-dioxane.

The crystallite sizes of SSE samples are slightly higher than those of DD samples according to the data evaluated by recalculating of FWHM value from the XRD patterns as given in Table 3. The higher peak intensity and crystallite size of SSE samples may be explained by Ostwald ripening occurring during solvent exchange.

Table 3. Crystallite sizes on the basis of Scherrer analysis of (311) XRD peaks

Proton Scavenger	Crystallite size* [nm]		Crystallite size [nm]		2θ for (311) peak [°]	
	DD	SSE	DD	SSE	DD	SSE
1,2-Epoxybutane	3.5	3.6	3.0	1.1	35.78	34.66
THF	3.0	3.2	1.3	3.3	35.37	34.83
1,4-Dioxane	3.5	3.7	2.9	3.1	34.94	35.14

* These data were evaluated by recalculating the full width at half maximum (FWHM) value from the XRD patterns rather than getting them directly from the XRD measurements

4.3 Thermal analysis

4.3.1 General characteristics

The thermal characteristics of Fe_2O_3 prepared by the DD and SSE methods were characterized in B/Fe_2O_3 nano-composites. TG/DSC heating curves for fuel rich B/Fe_2O_3 composites representing the equivalence ratio of 3 are presented in Figure 4.

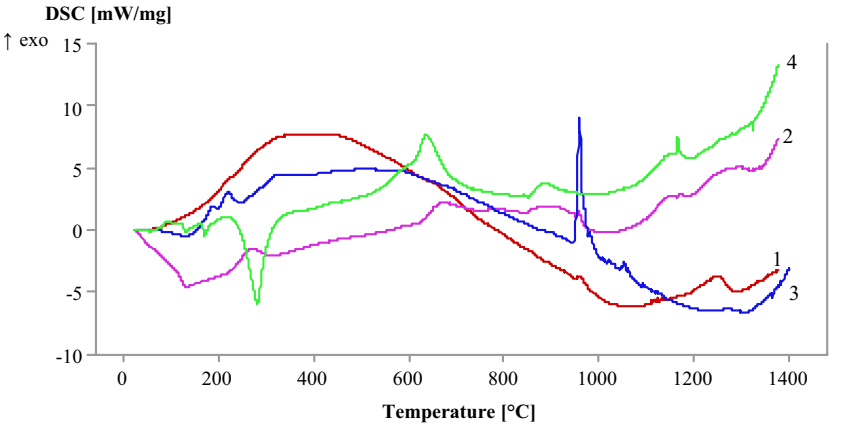

(a)

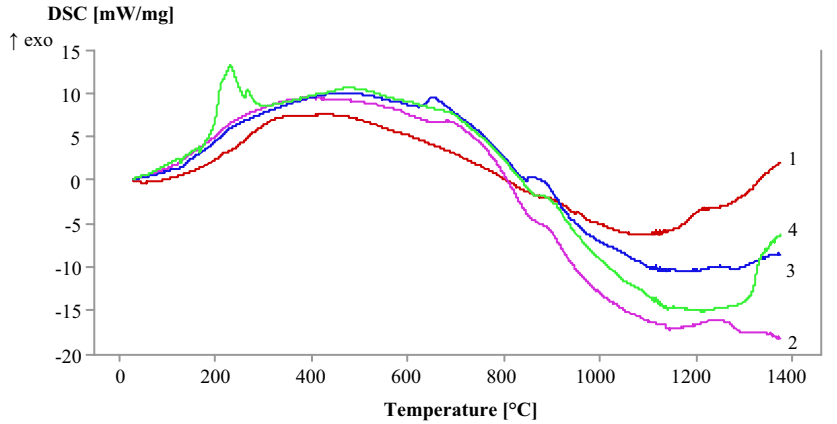

(b)

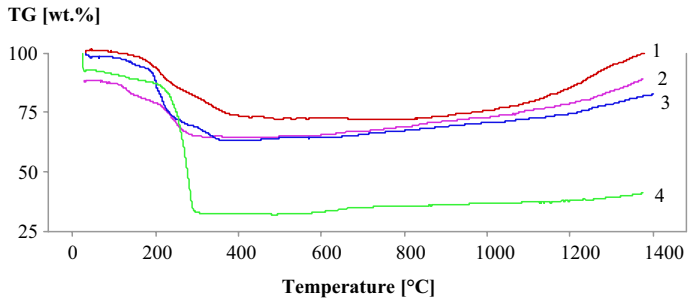

(c)

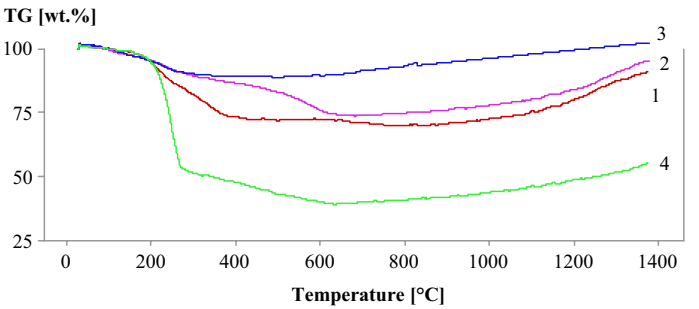

(d)

Figure 4. Plots as a function of temperature B/Fe_2O_3 samples synthesized with 1,2-epoxybutane (curve 1), THF (curve 2), 1,4-dioxane (curve 3) and ammonium hydroxide (curve 4) obtained in the DSC tests for: (a) DD and (b) SSE methods, as well as obtained in the TG tests for: (c) DD and (d) SSE methods

The samples prepared by different proton scavengers and obtained by the DD and SSE methods exhibited exothermic peaks across a broad range of temperatures. The melting temperature of boron is very high (2077 °C) and no endothermic peak was observed within the temperature range investigated. Therefore, the pyrotechnic reactions observed in the temperature range 600-1400 °C took place between solid phases of B and Fe_2O_3. The thermal events and mass loss of direct dried compositions up to 300 °C might be associated with the evaporation of the ethanol and organic residues inside the structure.

4.3.2 The effects of drying condition and proton scavenger on the thermal behavior of pyrotechnic compositions

The first exothermic events were observed above 850 °C for samples prepared using 1,2-epoxybutane. The exotherm of the SSE sample at 870 °C overlapped with an additional peak at a temperature slightly higher than 950 °C. The total heat output of the DD sample was 243.3 J/g while the total heat output of SSE sample was 354.6 J/g as given in Table 4 and Figures 4(a) and 4(b).

It is observed that the first exotherm above 600 °C for the DD composition prepared using THF had a heat output of 166.3 J/g at 629.3 °C while the first exotherm above 600 °C of SSE sample had a heat output of 496.9 J/g at 667.0 °C. When the results are compared for the exothermic events that took place above 600 °C, it can be seen that the onset temperatures of the exotherms of the SSE sample were slightly higher than those of the DD sample as shown in Figures 4(a) and 4(b). It was observed that the last exothermic event

Table 4. DSC data for B/Fe_2O_3 nano-composites

Proton Scavenger	1,2-epoxybutane		THF		1,4-dioxane		NH_4OH	
	DD	SSE	DD	SSE	DD	SSE	DD	SSE
Onset temp. 1 [°C]	–	–	238.2	–	159.2	–	–	198.3
Onset temp. 2 [°C]	–	–	–	–	–	–	–	455.2
Onset temp. 3 [°C]	–	–	629.3	667.0	572.9	639.3	542.7	642.6
Onset temp. 4 [°C]	950.6	873.4	848.7	870.0	867.7	855.1	851.9	864.5
Onset temp. 5 [°C]	1132.7	1117.9	1100.7	1188.9	1046.7	–	1095.7	–
Onset temp. 6 [°C]	–	–	1203.6	1302.6	–	1214.7	–	–
Heat output 1 [J/g]	–	–	78.7	–	185.9	–	–	631.6
Heat output 2 [J/g]	–	–	–	–	–	–	–	86.6
Heat output 3 [J/g]	–	–	166.3	496.9	12.2	336.8	696.6	82.8
Heat output 4 [J/g]	12.5	206.5	210.9	85.9	424.5	329.4	102.7	205.7
Heat output 5 [J/g]	230.8	148.1	511.9	605.9	–	–	162.3	–
Heat output 6 [J/g]	–	–	–	–	–	51.9	–	–
Total heat output [J/g]	243.3	354.6	967.8	1188.7	622.6	718.1	961.6	1006.7
Theoretical value [J/g]	–	–	1977		–	–	–	–

of the SSE sample started at 1188.9 °C with a heat output of 605.9 J/g and the last exothermic event of the DD sample started at 1100.7 °C with a heat output of 511.9 J/g. Another exotherm can be seen which overlaps the last exothermic event for both the SSE and DD samples. The onset temperature of this exotherm was 1302.6 °C for the SSE sample and 1203.6 °C for the DD sample. Similar to the results between 600-900 °C, the onset temperatures of the exothermic events above 1000 °C for the SSE sample were slightly higher than those of the DD sample. The total heat output of the DD sample was 967.8 J/g while the total heat output of the SSE samples was 1188.7 J/g as given in Figures 4(a) and 4(b).

The first exothermic event of the DD sample prepared using 1,4-dioxane had a heat output of 185.9 J/g at 159.2 °C. The exotherm above 600 °C for the DD composition had a heat output of 424.5 J/g at 867.7 °C which overlapped with the exotherm at 1046.7 °C while the first exotherm above 600 °C of the SSE sample had a heat output of 336.8 J/g at 639.3 °C and the second exotherm had a heat output of 329.4 J/g at 855.1 °C (see Figures 4(a) and 4(b)). The total heat output of the DD sample was 622.6 J/g while the total heat output of the SSE samples was 718.1 J/g.

The sharp endothermic peaks up to 250 °C observed for the DD samples prepared using ammonium hydroxide are given in Figure 4(a). The endothermic peaks between 50-150 °C correspond to the crystal transformation IV → III, III → II and II → I and the endothermic peaks above 150 °C may be related to the melting of residual ammonium nitrate [46, 47]. The NH_4NO_3 phase inside the structure may be produced during the gelation process with ammonium hydroxide according to the following possible reactions:

$$3NH_4OH + Fe(NO_3)_3 \rightarrow 3NH_4NO_3 + Fe(OH)_3 \quad (6)$$

$$Fe(OH)_3 \rightarrow FeOOH + H_2O \quad (7)$$

$$2FeOOH \rightarrow Fe_2O_3 + H_2O \quad (8)$$

The first exotherm was observed above 500 °C for the DD composition prepared using ammonium hydroxide with a heat output of 696.9 J/g at 542.7 °C while the first exotherm for the SSE sample was observed at 198.3 °C with a heat output of 631.6 J/g. When the results are compared for the exothermic events that took place above 650 °C, it can be seen that the onset temperature and heat output of the exotherm of the SSE sample are slightly higher than those of the DD sample as shown in Figures 4(a)

and 4(b). The last exothermic event of the DD sample started at 1095.7 °C with a heat output of 162.3 J/g which was not observed for the SSE sample. The total heat output of the DD sample was 961.6 J/g while the total heat output of SSE samples was 1006.7 J/g.

The onset temperatures of the SSE samples prepared using THF, 1,4-dioxane and ammonium hydroxide were slightly higher than those of the DD samples. Wang *et al.* [48] proposed that pyrotechnic ignition is controlled by the transport of bound oxygen ions from the oxidizer and is related to the internal structure of the oxidizer [49]. Therefore, the difference in the onset temperatures of the SSE and DD iron oxide xerogels may be attributed to slight differences in the structure, such as vacancies, defects and oxygen bonds.

The heat outputs of the SSE samples were approximately 5-45% greater than the heat outputs of the DD samples prepared using 1,2 epoxybutane, THF, 1,4-dioxane and ammonium hydroxide (see Table 4). The enhancement of the heat output might be related to the textural properties of the samples which strongly depend on the drying conditions as the drying method is known to affect the mechanism of extraction/evaporation of the solvent within the porous structure of gel.

The theoretical and experimental values of the heat of reactions for the 3FR both SSE and DD samples are shown in Table 4. The actual calorific values are approximately 15-60% of the theoretical values. It can be concluded that the SSE method has an enhancing effect on the heat output due to enhancement in the structure, the increase in the surface area and pore volume. It can be seen that the heat output not only depends on the drying conditions but also strongly depends on the type of proton scavenger. The highest heat outputs were obtained with samples prepared using THF and ammonium hydroxide. Despite the lowest surface area occurred for the sample prepared using ammonium hydroxide, it had an enhancing effect on the heat output. This may be related with ammonium nitrate obtained during the gelation process. It is known that ammonium nitrate has an enhancing effect on heat output due to it being a strong oxidizing agent for boron powder. On the other hand, samples prepared using 1,2-epoxybutane had the highest surface area. However, 1,2-epoxybutane may inhibit the ignition conditions of the B/Fe_2O_3 as it is more stable compared to other proton scavengers.

5 Conclusions

Energetic nano-composites of boron and iron oxide xerogels synthesized using THF, 1,4-dioxane and ammonium hydroxide are promising materials for pyrotechnic compositions. Moreover, the sequential solvent exchange method improves the crystallinity and textural properties of Fe_2O_3 which also enhances the thermal properties of B/Fe_2O_3 pyrotechnics. The sequential solvent exchange samples prepared using ammonium hydroxide and THF had the highest total heat output (more than 1000 J/g) of all the compositions studied.

The results show that the structural properties of Fe_2O_3 xerogels are strongly affected by the type of proton scavenger used. The highest surface area was obtained using 1,2-epoxybutane and 1,4-dioxane. The results also indicate that the proton scavengers affect not only the surface area but also the thermal behavior of the B/Fe_2O_3 composites. From the material characterization point of view, 1,2-epoxybutane and 1,4-dioxane are the most promising proton scavengers to improve the structural behavior of xerogels by increasing the surface area. On the other hand, from the thermal behavior point of view; ammonium hydroxide and THF are the most promising proton scavengers to enhance the total heat output of the nano-composites.

The iron oxide with a mesoporous structured matrix can be derived by utilizing all the proton scavengers mentioned above. It is possible to adjust the structural and thermal behavior of the B/Fe_2O_3 xerogels by varying the synthesis and drying conditions.

Acknowledgements

We would like to thank Material Characterization Laboratory of Roketsan Inc. and Central Laboratory of Middle East Technical University. This study is funded by Roketsan Inc.

References

[1] Staley, C.S.; Morris, C.J.; Thiruvengadathan, R.; Apperson, S.J.; Gangopadhyay, K.; Gangopadhyay S. Silicon-based Bridge Wire Micro-chip Initiators for Bismuth Oxide-Aluminum Nanothermite. *J. Micromech. Microeng.* **2011**, *21*: 115015.

[2] Zhang, K.L.; Choua, S.K.; Ang, S.S.; Tang, X.S. A MEMS-based Solid Propellant Microthruster with Au/Ti Igniter. *Sens. Actuators, A* **2005**, *122*: 113-123.

[3] Martirosyan, K.S.; Wang, L.; Vicent, A.; Luss, D. Nanoenergetic Gas-generators: Design and Performance. *Propellants Explos. Pyrotech.* **2009**, *34*, 532-538.

[4] Brinker, C.J.; Scherer, G.W. *Sol-Gel Science.* Academic Press, Boston, **1990**; ISBN 978-0-12-134970-7.
[5] Schoenitz, M.; Ward, T.S.; Dreizin E.L. Fully Dense Nano-composite Energetic Powders Prepared by Arrested Reactive Milling. *Proc. Combust. Inst.* **2005**, *30*: 2071-2078.
[6] Tillotson, T.M.; Gash, A.E.; Simpson, R.L.; Hrubesh, L.W.; Satcher, J.H. (Jr.); Poco, J.F. Nanostructured Energetic Materials Using Sol-gel Methodologies. *J. Non-Cryst. Solids* **2001**, *285*: 338-345.
[7] Clapsaddle, B.J.; Zhao, L.; Prentice, D.; Pantoya, M.L.; Gash, A.E.; Satcher, J.H. (Jr.); Shea, K.J.; Simpson, R.L. Formulation and Performance of Novel Energetic Nanocomposites and Gas Generators Prepared by Sol-Gel Methods. *ICT Ann. Conf., Proc., 36th,* Karlsruhe, Germany, **2005**.
[8] Walker, J.; Tannenbaum, R. Formation of Nanostructured Energetic Materials *via* Modified Sol-Gel Synthesis. *MRS Proc.* **2003**, *800:* AA7.8.1-AA7.8.10.
[9] Prakash, A.; McCormick, A.V.; Zachariah, M.R. Tuning the Reactivity of Energetic Nanoparticles by Creation of a Core-Shell Nanostructure. *Nano Lett.* **2005**, *5*(7): 1357-1360.
[10] Malchi, J.Y.; Foley, T.J.; Yetter, R.A. Electrostatically Self-Assembled Nanocomposite Reactive Microspheres. *ACS Appl. Mater. Interf.* **2009**, *1*(11): 2420-2423.
[11] Kim, S.H.; Zachariah, M.R. Enhancing the Rate of Energy Release from Nanoenergetic Materials by Electrostatically Enhanced Assembly. *Adv. Mater.* **2004**, *16*: 1821-1825.
[12] Churaman, W.A.; Currano, L.J.; Becker, C. Initiation and Reaction Tuning of Nanoporous Energetic Silicon. *J. Phys. Chem. Solids* **2010**, *71*: 69-74.
[13] Churaman, W.A.; Becker, C.R.; Metcalfe, G.D.; Hanrahan, B.M.; Currano, L.J.; Stoldt, C.R. Optical Initiation of Nanoporous Energetic Silicon for Safing and Arming Technologies. *Optical Technologies for Arming, Safing, Fuzing, and Firing* VI, Vol. 7795, **2010**.
[14] Currano, L.J.; Churaman, W.A. Energetic Nanoporous Silicon Devices. *J. Microelectromech. Sys.* **2009**, *18*: 799-807.
[15] Feynman, R.P. *There's Plenty of Room at the Bottom.* American Physical Society, Pasadena, **1959**.
[16] Goldschmidt, H.; Weil, O. *Method of Manufacturing Metals.* Patent US 895, **1908**.
[17] Livage, J.; Henry, M.; Sanchez, C. Sol-gel Chemistry of Transition Metal Oxides. *Prog. Solid State Chem.* **1988**, *18*: 259-341.
[18] Cornell, R.M.; Schwertmann, U. *The Iron Oxides: Structure, Properties, Reactions, Occurrences and Uses.* Wiley-VCH, Weinheim, **2003**.
[19] Jolivet, J.P.; Henry, M.; Livage, J. *Metal Oxides Chemistry and Synthesis: From Solution to Solid State.* John Wiley & Sons, Chichester, **2000**.
[20] Son, S.F.; Yetter, R.A.; Yang, V. Introduction: Nanoscale Composite Energetic Materials. *J. Propul. Power* **2007**, *23:* 643.

[21] Aegerter, M.A.; Leventis, N.; Koebel, M.M. *Aerogels Handbook: Advances in Sol-gel Derived Materials and Technologies.* Springer, New York, **2011**.
[22] Pantoya, M.L.; Granier, J.J. Combustion Behavior of Highly Energetic Thermites: Nano versus Micron Compositions. *Propellants Explos. Pyrotech.* **2005**, *30*(1): 53-62.
[23] Shimojo, F.; Nakano, A.; Kalia, R.K.; Vashishta, P. Electronic Processes in Fast Thermite Chemical Reactions: A First-principles Molecular Dynamics Study. *Phys. Rev. E* **2008**, *77*: 066103.
[24] Levitas, V.I.; Asay, B.W.; Son, S.F.; Pantoya, M. Melt Dispersion Mechanism for Fast Reaction of Nanothermites. *Appl. Phys. Lett.* **2006**, *89*: 071909.
[25] Danen, W.C.; Martin, J.A. *Energetic composites.* Patent US 5266132, **1993**.
[26] Thiruvengadathan, R.; Bezmelnitsyn, A.; Apperson, S.; Staley, C.; Redner, P.; Balas, W.; Nicolich, S.; Kapoor, D.; Gangopadhyay, K.; Gangopadhyay, S. Combustion Characteristics of Novel Hybrid Nanoenergetic Formulations. *Combust. Flame* **2011**, *158*: 964-978.
[27] Brown, M.E.; Taylor, S.J.; Tribelhorn, M.J. Fuel-oxidant Particle Contact in Binary Pyrotechnic Reactions. *Propellants Explos. Pyrotech.* **1998**, *23*: 320-327.
[28] Kofstad, P. *High-Temperature Oxidation of Metals.* Wiley, New York, **1966**.
[29] Prentice, D.; Pantoya, M.L.; Clapsaddle, B.J. Synthesis and Performance Characterization of a Nanocomposite Ternary Thermite: Al/Fe_2O_3/SiO_2. LLNL, UCRL-JRNL-209471, **2005**.
[30] HSC Chemistry: Version 9.0.1, Qutotec, Research Center, Finland.
[31] Brunauer, S.; Deming, L.S.; Deming, W.E.; Teller, E. On a Theory of van der Waals Adsorption of Gases. *J. Am. Chem. Soc.*, **1940**, *62*: 1723.
[32] Rouquerol, F.; Rouquerol, J.; Sing, K. *Adsorption by Powders and Porous Solids*. Academic Press, London, **1999**.
[33] Sing, K.S.W.; Everett, D.H.; Haul, R.A.W.; Moscou, L.; Pierotti, R.A.; Rouquerol, J.; Siemieniewska, T. Reporting Physisorption Data for Gas/Solid Systems with Special Reference to the Determination of Surface Area and Porosity. *Pure Appl. Chem.* **1985**, *57*(4): 603-619.
[34] Serna, C.J.; Morales, M.P. Maghemite (γ-Fe_2O_3): A Versatile Magnetic Colloidal Material. *Surf. Colloid Sci.* **2004**, *17*: 27-81.
[35] Ferguson, A.; Hass, M. Magnetic Structure and Vacancy Distribution in γ-Fe_2O_3 by Neutron Diffraction. *Phys. Rev. Lett.* **1958**, *112*: 1130.
[36] Setvin, M.; Wagner, M.; Schmid, M.; Parkinson, G.S.; Diebold, U. Surface Point Defects on Bulk Oxides: Atomically-resolved Scanning Probe Microscopy. *Chem. Soc. Rev.* **2017**, *46*: 1772.
[37] Van der Steen, A.C.; Verbeek, H.J.; Meulenbrugge, J.J. Influence of RDX Crystal Shape on the Shock Sensitivity of PBXs. *Symp. Det., Proc., 9th,* Portland, OR, **1989**, *83*.
[38] Borne, L. Influence of Intragranular Cavities of RDX Particle Batches on the Sensitivity of Cast Wax Bonded Explosives. *Symp. Det., Proc., 10th,* Boston, MA, **1993**, *286*.

[39] Baer, M.R. Modeling Heterogeneous Energetic Materials at the Mesoscale. *Thermochim. Acta* **2002**, *384*: 351-367.
[40] Morales, M.P.; Pecharroman, C.; González-Carreño, T.; Serna, C.J. Structural Characterisation of Uniform γ-Fe_2O_3 Particles with Different Axial (Length/Width) Ratios. *J. Solid State Chem.* **1994**, *108*, 158-16.
[41] Morales, M.P.; de Julián, C.; González, J.M.; Serna, C.J. The Effect of Vacancies Distribution on the Magnetic Properties of γ-Fe_2O_3 Particles. *J. Mater. Res.* **1994**, *9*, 135-141.
[42] Morales, M.P.; Serna, C.J.; Bødker, F.; Mørup, S. Spin-Canting Due to Structural Disorder in Maghemite. *J. Phys.: Condens. Matter* **1997***, 9*: 5461-5467.
[43] Bastow, T.J.; Trinchi, A.; Hill, M.R.; Harris, R.; Muster, T.H. Vacancy Ordering in γ-Fe_2O_3 Nanocrystals Observed by ^{57}Fe NMR. *J. Magn. Magn. Mater.* **2009**, *321*: 2677-2681.
[44] Scherrer, P. Bestimmung der Grösse und der inneren Struktur von Kolloidteilchen mittels Röntgenstrahlen. (in German) *Nachr. Ges. Wiss. Göttingen*, **1918**, *26*: 98-100.
[45] Langford, J.I.; Wilson, A.J.C. Scherrer after Sixty Years: A Survey and Some New Results in the Determination of Crystallite Size. *J. Appl. Cryst.* **1978**, *11*: 102-113.
[46] Rasulic, G.; Jovanovic, S.; Milanovic, L. Ammonium Nitrate Changes during Thermal Analysis. *J. Therm. Anal.* **1985**, *30*: 65-72.
[47] Chaturvedi, S.; Dave, P.N. Review on Thermal Decomposition of Ammonium Nitrate. *J. Energ. Mater.* **2013**, *31*: 1-26.
[48] Wang, X.; Zhou, W.; DeLisio, J.B.; Egan, G.C.; Zachariah, M.R. Doped δ-Bismuth Oxides to Investigate Oxygen Ion Transport as a Metric for Condensed Phase Thermite Ignition. *J. Phys. Chem.* **2017**, *121*: 147-152.
[49] Boyapati, S.; Wachsman, E.D.; Jiang, N. Effect of Oxygen Sublattice Ordering on Interstitial Transport Mechanism and Conductivity Activation Energies in Phase-stabilized Cubic Bismuth Oxides. *Solid State Ionics* **2001**, *140*(1): 149-160.

Received: July 31, 2019
Revised: March 9, 2020
First published online: March 20, 2020